geosciences

MDPI

Article

Asbestos Hazard in Serpentinite Rocks: Influence of Mineralogical and Structural Characteristics on Fiber Potential Release

Lorenzo Marzini [1,*], Marco Iannini [2], Giovanna Giorgetti [3], Filippo Bonciani [4], Paolo Conti [2], Riccardo Salvini [2] and Cecilia Viti [3,*]

1 Institute of Applied Physics "Nello Carrara" (IFAC), National Research Council (CNR), 50019 Sesto Fiorentino, Italy
2 Department of Environment, Earth and Physical Sciences and Centre of Geotechnologies CGT, University of Siena, Via Vetri Vecchi 34, 52027 San Giovanni Valdarno, Italy; geolmarcoiannini@gmail.com (M.I.); paolo.conti@unisi.it (P.C.); riccardo.salvini@unisi.it (R.S.)
3 Department of Physical, Earth and Environmental Sciences, University of Siena, 53100 Siena, Italy; giovanna.giorgetti@unisi.it
4 CGT Engineering S.r.l., Via Strasburgo 7, 52022 Cavriglia, Italy; bonciani@unisi.it
* Correspondence: marzini4@student.unisi.it (L.M.); cecilia.viti@unisi.it (C.V.)

Abstract: Naturally occurring asbestos (NOA) represents a matter of social and environmental concern due to its potential release in the atmosphere during rock excavation and grinding in quarry and road tunnel activities. In most cases, NOA occurs in serpentinites, i.e., rocks deriving from low-grade metamorphic hydration of mantle peridotites. The potential release of asbestos fibers from serpentinite outcrops depends on several features, such as serpentinization degree, rock deformation, weathering, and abundance of fibrous veins. In this study, we selected a set of serpentinite samples from a representative outcrop in Tuscany (Italy), and we analyzed them by Optical, Scanning, and Transmission Electron Microscopies. The samples were treated by grinding tests following the Italian guidelines Decrees 14/5/96 and 152/2006 for the determination of the Release Index (RI), i.e., the fiber amount released through controlled crushing tests. The fine-grained powder released during the tests was analyzed by quantitative Fourier transform infrared spectroscopy (FTIR) to determine the variety and the amount of released fibers and to assess the potential hazard of the different serpentinite samples. Results indicate that the amount of released fibers is mostly related to serpentinite deformation, with the highest RI values for cataclastic and foliated samples, typically characterized by widespread occurrence of fibrous veins. Conversely, massive pseudomorphic serpentinite revealed a very low RI, even if their actual chrysotile content is up to 20–25%. Based on our original findings from the RI results, a preliminary investigation of the outcrop at the mesoscale would be of primary importance to obtain a reliable hazard assessment of NOA sites, allowing the primary distinction among the different serpentinites lithotypes and the effective fiber release.

Keywords: asbestos; NOA; serpentinites; fibrous vein; abrasion tests; release index; FTIR

check for updates

Citation: Marzini, L.; Iannini, M.; Giorgetti, G.; Bonciani, F.; Conti, P.; Salvini, R.; Viti, C. Asbestos Hazard in Serpentinite Rocks: Influence of Mineralogical and Structural Characteristics on Fiber Potential Release. *Geosciences* **2024**, *14*, 210. https://doi.org/10.3390/geosciences14080210

Academic Editor: Ian Coulson

Received: 5 July 2024
Revised: 31 July 2024
Accepted: 3 August 2024
Published: 5 August 2024

Copyright: © 2024 by the authors. Licensee MDPI, Basel, Switzerland. This article is an open access article distributed under the terms and conditions of the Creative Commons Attribution (CC BY) license (https://creativecommons.org/licenses/by/4.0/).

1. Introduction

The term "asbestos" refers to a group of silicate minerals, in particular chrysotile $Mg_3Si_2O_5(OH)_4$, the fibrous variety of serpentine, and five amphiboles: grunerite $(Fe,Mg)_7Si_8O_{22}(OH)_2$ (commercial name amosite), riebeckite $Na_2(Fe,Mg)_5Si_8O_{22}(OH)_2$ (commercial name crocidolite), anthophyllite $(Mg,Fe)_7Si_8O_{22}(OH)_2$, tremolite $Ca_2Mg_5Si_8O_{22}(OH)_2$, and actinolite $Ca_2(Mg,Fe)_5Si_8O_{22}(OH)_2$. Asbestos minerals have fibrous habit (i.e., lower than 3 µm in diameter and more than 5 µm in length) and are characterized by unique physical, chemical, and mechanical properties. Their unique properties explained the past extensive use of asbestos in a wide range of applications (e.g., [1–4]). Asbestos has been widely used in construction industries due to physical properties such as sound absorption

and thermal insulation (e.g., [1,5]). Cement–asbestos is a composite material where asbestos fibers are included within a cement matrix, and it has been extensively used in roofing and other building components (e.g., [6–8]). Asbestos has been also used in plastic materials and in the textile industry as a structural stability agent [9].

The huge and widespread occurrence of asbestos-containing materials and, subsequently, of related wastes (ACM and ACW, respectively) now represents a serious environmental and health problem, since it is well known that the inhalation of asbestos fibers is responsible for asbestosis and pleural cancer (e.g., [10–17]). Asbestos use has been therefore regulated and/or banned in many countries by the International Ban Asbestos Secretariat, and main efforts are now dedicated to accurate monitoring of potentially harmful occurrences and to ACM/ACW safe management. The potential hazard of specific occurrences and samples can be evaluated by (1) quantitative determination of airborne particulate, following the procedures of [18], which is mostly applied to the case of potentially exposed workers, and (2) quantitative determination of asbestos content in massive samples [19]. In the case of the industrial materials (both ACM and ACW), the identification and the quantification of asbestos fibers does not pose any analytical problem since the fibers are chemically and mineralogically distinct from the matrix in which they are included (for example a Ca-silicatic cement or a polymeric matrix).

The main problem in ACM and ACW management is represented by the enormous volumes involved, which require complex and costly treatments and/or removal and disposal in controlled landfills. However, we must keep in mind that asbestos fibers may also occur in natural occurrences [20–24]. The study of massive rocks is more complex than synthetic ACM, and even a correct fiber identification may be complicated by intrinsic difficulties, arising from analytical resolution limits and from typical mineralogical–microstructural characteristics of asbestos-bearing rocks. The Italian Ministerial Decree of 14 May 1996 [19] reports a list of asbestos-bearing rocks and defines the procedures for monitoring and risk assessment of naturally occurring asbestos (NOA) sites. Serpentinites are the most common lithologies hosting asbestos fibers (chrysotile and, subordinately, tremolite, anthophyllite, and/or actinolite amphiboles), finely intermixed with the equivalent non-fibrous phases. As an example, a massive retrograde serpentinite, with typical mesh and bastite pseudomorphic textures, is formed by a nanoscale mixture of chrysotile fibers and lizardite lamellae, together with polygonal and polyhedral serpentine (e.g., [25–29]). This complex nanostructure, with fibrous and non-fibrous serpentines finely intergrown, may severely complicate an accurate identification of the different serpentine polymorphs.

Optical polarizing microscopy and scanning electron microscopy (SEM) are relatively fast and easy methods; in most cases, they provide a reliable asbestos identification, but their resolution limits hamper an accurate and precise quantification of asbestos fibers. Chemical approaches (such as X-ray spectroscopy coupled with SEM) are also failing, as the compositional differences between chrysotile and non-fibrous serpentines are minimal, and they are lost when analyzing mixed, polymineralic volumes [24]. Conventional X-ray diffraction methods do not provide unequivocal answers in the case of bulk serpentinite samples [30], as well. As a matter of fact, the differences in diffraction patterns of lizardite and chrysotile (possibly complicated by the concomitant occurrence of polygonal and polyhedral serpentine) are very subtle and are lost when analyzing a polyphasic bulk sample. The only successful technique would be transmission electron microscopy (TEM), whose spatial resolution allows the detection of nano-sized serpentine fiber and crystals/lamellae [31]. Unfortunately, TEM cannot be considered as a routine technique for the identification (and quantification) of asbestos fibers, being considerably complex and time-consuming. Promising analytical perspectives for fiber identification as well as for quantitative purposes are represented by Raman and Infrared spectroscopies [32–38] and thermal analysis [39–41]. These methods seem to be successful in serpentine polymorphs' discrimination, allowing the obtainment of calibration curves using controlled mixtures of chrysotile + lizardite and chrysotile + antigorite standards, and providing relatively accurate quantitative estimates of the chrysotile content [40].

Some authors suggest a different approach to NOA hazard assessment, based on the hypothesis that the fiber content (and their potential release) in massive, undeformed samples rarely exceeds the contamination threshold for the Italian laws [42]. Giacomini et al. [21], Labagnara et al. [43], and Gaggero et al. [22] report quantitative field survey and geomechanical analyses of shear zones, fracture, and vein occurrences in Ligurian ophiolite outcrops, indicating possible analytical protocols for asbestos reliable estimations in natural occurrences and samples. The key feature when dealing with NOA is not the actual fiber content but the effective fiber release, especially during excavation and grinding processes in quarries, roads, and tunnels (e.g., [21,22,43]). The abovementioned Decree 14/5/96 [19] also introduced the Release Index (RI), which indicates the number of fibers released by natural massive samples during controlled mechanical wear tests [44]. However, no release test data are available to date. For this purpose, we performed an RI test on a selected set of serpentinite samples from Tuscany (Italy), characterized by different microstructures and variable deformation extent, aiming to (a) find a correlation between field/petrographic evidence and actual asbestos release and (b) suggest a reliable strategy for risk assessment in the complex case of natural occurrences. This work aims therefore to contribute and strengthen the multi-analytical approach from the field to the lab scale. Indeed, in our opinion the multi-analytical approach represents the most reliable way to assess the actual asbestos hazard of specific natural occurrences, combining engineering-geological and laboratory expertise.

2. Materials and Methods

2.1. Geological Occurrence and Serpentinite Samples

The study area is located in the eastern part of the Tuscany Region (Italy), into the surroundings of the Rognosi Mounts, Arezzo province (Figure 1). The Rognosi Mounts represent the product of the NE-verging Northern Apennines fold and thrust belt developed because of Cenozoic collision between the Corso–Sardinian block and the Adriatic plate [45,46]. In particular, the Ligurian Units are allochthonous terrains scraped off from Alpine Tethys oceanic crust, and they correspond to the uppermost tectonic units in the Apennine nappe pile. These units were thrusted from west to east over the developing thrust wedge, which progressively incorporated tectonic units deposited as Miocene siliciclastic turbidite sequences in the Adriatic foredeep [47,48]. Consequently, the Ligurian Units are tectonically superposed onto the Miocene turbidites, which, in the study area, are represented by the Falterona Sandstones. The geology of the study area includes Middle Jurassic–Lower Cretaceous magmatic and sedimentary rocks [49,50]. This unit includes peridotites, gabbro dykes, basalts, and ophiolitic breccias that are overlain by Upper Jurassic radiolarite (Diaspri Formation Auct.), Lower Cretaceous Calpionella Limestone, and Palombini Shale Formations, the latter grading upwards into the Aptian to Eocene Sillano Formation, in turn followed by the Eocene Monte Morello Formation. This stratigraphic succession continues with the Argille Varicolori Formation and ends with the Monte Senario Sandstone Formation, testifying the foredeep evolution of the sedimentary basin [50]. In the present study, we carefully analyzed and sampled 15 different serpentinite outcrops, as reported in Figure 1. The investigated samples (name, lithotype, and experimental determinations) are shown in Table 1. Ten samples (from "1S" to "10S"), located in the Coreca area (Calabria Region, Italy), are used for comparison (Figure 2). In this area, the Apennine Unit (Triassic dolostone and dolomitic limestone) is overthrusted by the ophiolitic sequences (belonging to Gimigliano-Monte Reventino Units) [51,52]. Calabrian samples belong to the Gimigliano-Monte Reventino Units, consisting of serpentinites, metabasalts, metagabbros/metadolerites with a metasedimentary cover represented by a sequence of marble and calcschists and quarzites [53,54]. The metamorphic units are sealed by the Miocene sedimentary sequences consisting of calcareous sandstones, calcarenites, clays, marls, and Messinian limestone ("Calcare di base"). Pleistocene terraced deposits, consisting of conglomerates and sands, outcrop at the top of the succession [51].

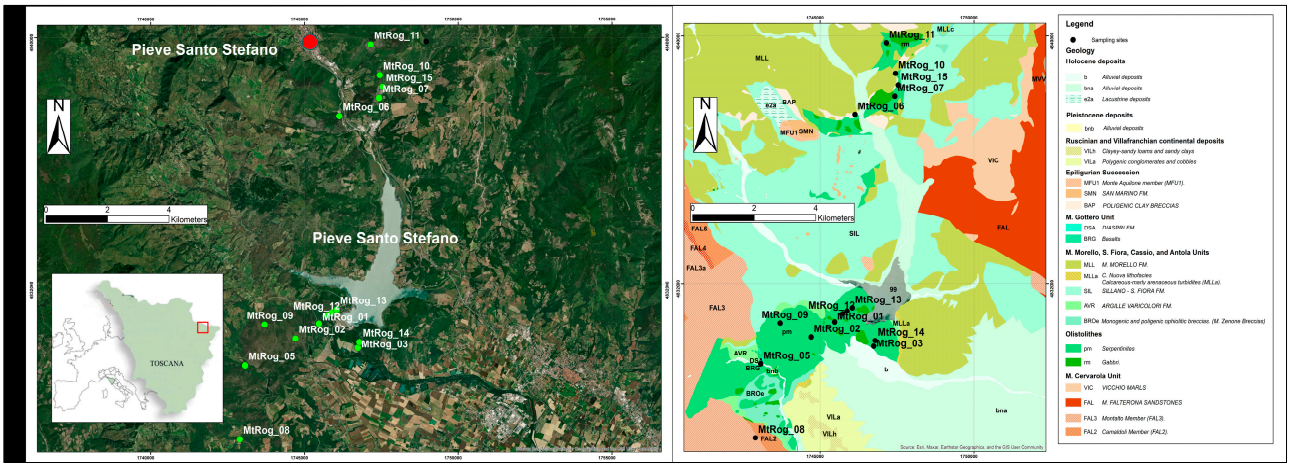

Figure 1. Serpentinite outcrops, sample location (coordinate system: Gauss-Boaga, west zone) and geological map (adapted from Db Geologico Regionale [55]).

Table 1. List of samples and corresponding analyses. Asbestos quantification after wear tests has been determined by FTIR and SEM counting, for the Monti Rognosi and Calabria samples, respectively.

#	Sample	Lithotype	Optical Microscopy	SEM/EDS	Wear Test and FTIR Analysis or SEM Counting
1	MtRog_01	Massive serpentinite	X	X	X
2	MtRog_02	Cataclasite	X	X	X
3	MtRog_03	Massive serpentinite	X	X	X
4	MtRog_04	Cataclasite	X	X	X
5	MtRog_05	Serpentine veins	X	X	X
6	MtRog_06	Serpentine veins	X		X
7	MtRog_07	Cataclasite	X	X	X
8	MtRog_08	Serpentine veins	X		X
9	MtRog_09	Massive serpentinite	X		X
10	MtRog_10	Serpentine veins	X		X
11	MtRog_11	Massive serpentinite	X		X
12	MtRog_12	Massive serpentinite	X	X	
13	MtRog_13	a = massive serpentinite (dunitic protolith); b = massive serpentinite; c = foliated serpentinite with pseudofibrous vein	X	X	
14	MtRog_14	a = massive serpentinite; b = antigorite and tremolite veins; c = foliated serpentinite with sigmoidal chrysotile veinlets	X	X	
15	MtRog_15	a = massive serpentinite; b = cataclasite; c = splintery antigorite vein	X	X	
16	1S	Massive serpentinite	X	X	X
17	2S	Massive serpentinite	X	X	X
18	3S	Massive serpentinite	X	X	X
19	4S	Massive serpentinite	X	X	X
20	5S	Massive serpentinite	X	X	X
21	6S	Massive serpentinite	X	X	X
22	7S	Massive serpentinite	X	X	X
23	8S	Massive serpentinite	X	X	X
24	9S	Massive serpentinite	X	X	X
25	10S	Massive serpentinite	X	X	X

The Monti Rognosi outcrops allow a wide variety of serpentinite lithotypes to be investigated, characterized by different serpentinization degree, weathering, and deformation

extent and mechanism. The first lithotype is represented by typical massive serpentinites (MS in Figure 3), unaffected by deformation and weathering processes. MS samples consist of a fine-grained, dark green matrix with pale green lamellae up to 5 cm wide in size, corresponding to mesh and bastite retrograde pseudomorphic textures after olivine and pyroxene, respectively. In some outcrops, bastites are absent, suggesting local dunitic protoliths. From a mineralogical point of view, meshes consist of lizardite-rich rims and cores, these last formed by a random ultrafine association of lizardite lamellae, chrysotile and polygonal serpentine fibers, and poorly crystalline serpentine. This ultrafine association of different serpentine varieties also occurs in bastite lamellae.

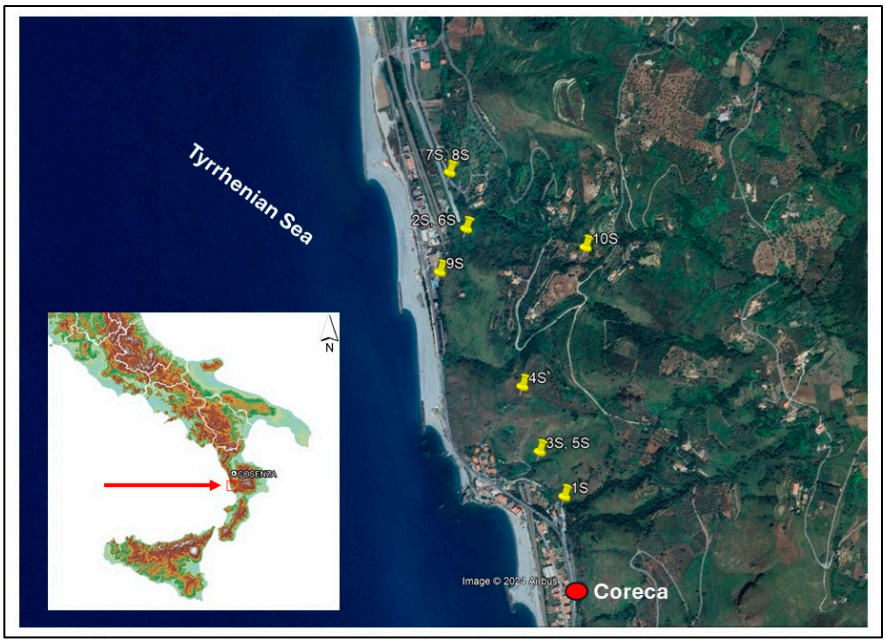

Figure 2. Calabrian massive serpentinite samples location (image from Google Earth).

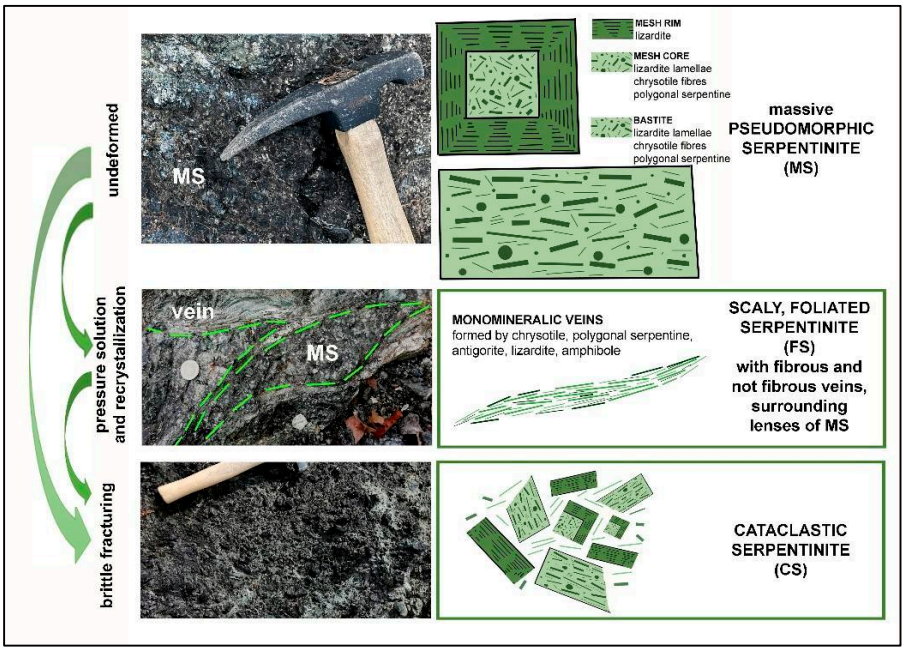

Figure 3. Main lithotypes in serpentinitic outcrops: massive, undeformed serpentinites (MS) with mesh and bastite pseudomorphic textures; foliated serpentinites (FS), formed by pressure solution and subsequent dynamic precipitation of new serpentines in fibrous/pseudofibrous veins; cataclastic serpentinites (CS), dominated by brittle fracturing and grain size reduction.

The second lithotype is represented by scaly, foliated serpentinites (FS in Figure 3), characterized by lens-shaped bodies of dark green massive serpentinite MS (from meter to millimeter in size), surrounded by pale green, fibrous, and splintery serpentine veins. Foliated serpentines result from deformation processes dominated by pressure solution mechanisms mostly involving mesh cores [56], followed by precipitation of fibrous and pseudofibrous serpentines in shear corridors and veins. Serpentine veins and envelopes may consist of fibrous chrysotile (i.e., asbestos), polygonal serpentine, or antigorite (i.e., serpentine varieties that are not classified as asbestos minerals), and rarely, fibrous amphibole (i.e., asbestos). The third lithotype corresponds to serpentinites deformed with a predominant brittle cataclastic mechanism (CS in Figure 3). Both MS and FS lithotypes may be involved in cataclastic fracturing, resulting in poorly coherent samples, with random clasts of MS, FS, and serpentine veins, embedded within a fine-to-ultrafine serpentine matrix.

2.2. Release Index Determination: Experimental Details

Mechanical stresses during handling operations and excavation were simulated using a mechanical apparatus, which allows the production of fine particles from the chipping and the abrasion processes on the rock materials [23]. In detail, following the Italian legislation [19], grinding tests were carried out using a mechanical apparatus consisting of a steel rotary cylinder with a diameter of 300 mm, an axial length of 400 mm, and a rotation speed equal to 50 rpm [57] (Figure 4). Rock samples for the grinding test were prepared following the Italian legislation guidelines (stone fragments with size of 5–50 mm, sample weight equal to 0.5 kg), and the self-milling duration was set to 4 h. Upon completion of the grinding test, the material was filtered (sieve pass equal to 1 mm) and oven-dried for 12 h at 105 °C. All the steps of the analysis procedure, such as the selection of the sample, rock fragments preparation, extraction of the grinding material from the apparatus, sample filtration, and the drying phase, were carried out using adequate protection devices and under a fume hood, to prevent the operator from the exposure to asbestos fibers.

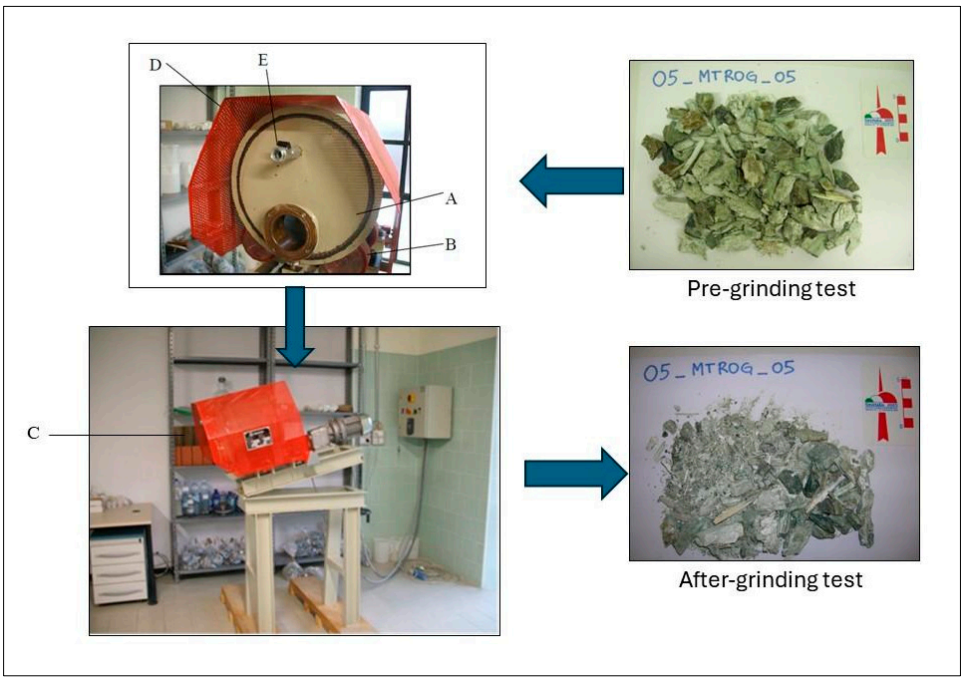

Figure 4. Grinding test mechanical apparatus scheme: (A) steel cylinder; (B) rotating rollers; (C) tilting of the cylinder through the hand screw; (D) security grid; (E) faucet with valve.

2.3. FTIR Method for Asbestos Quantification

FTIR analysis was carried out on reference samples (e.g., tremolite, serpentine polymorphs: chrysotile, antigorite, lizardite), on mixtures of the reference samples with known

concentrations, and on selected serpentinites from the Monti Rognosi outcrops (Table 1). Data were obtained by a Spectrum 100 FTIR spectrometer (PerkinElmer, Waltham, MA, USA) using a mixture of powdered sample (obtained after the grinding test) and KBr in a ratio of about 3:300. The sample/KBr mixture was put into a steel cylinder and placed under a press (10 tons) for about 5 min, obtaining compact and transparent pellets [58,59]. Before data acquisition, the pellets were kept in an oven overnight (at approximately 100 °C) to eliminate adsorbed atmospheric humidity. Semi-quantitative assessment of asbestos concentrations in NOA samples was carried out through the application of calibration curve method [60], applied to the most suitable IR peaks (e.g., OH stretching signals; [61]).

3. Results

3.1. Petrographic Description of Massive, Foliated, and Cataclastic Serpentinites

Under polarizing microscope, MS revealed typical retrograde pseudomorphic textures. Serpentinization starts along olivine microcracks, with the crystallization of lizardite "columns" (grey rims in Figure 5a), oriented perpendicular to the rim boundary, and of magnetite (opaque micrograins in Figure 5a, aligned along the rim boundaries). The orientation of lizardite columnar crystals is responsible for the typical "wavy" extinction of rims. Mesh cores (Figure 5b), deriving from successive fast hydration, are microgranular or cryptocrystalline, being formed by fine–ultrafine random association of different serpentine varieties (both fibrous and non-fibrous). As stated above, this complex ultrafine association occurs also in bastitic lamellae (arrow in Figure 5c), deriving from ortho- and clinopyroxene crystals. In most cases, peridotitic minerals are completely replaced by serpentine minerals, except for some patches where abundant relics of olivine (yellow cores in Figure 5a), ortho- and clinopyroxenes are still preserved, together with spinel anhedral grains. Figure 5c shows an example of hourglass texture, i.e., a sort of mesh texture in which cores were not formed: olivine serpentinization resulted only in columnar lizardite crystallization, whose orientation is responsible for the characteristic "hourglass" extinction mode.

For the purposes of this study, it is remarkable that chrysotile fibers are widespread also in massive serpentinites, within mesh cores and bastites, up to approximately 25% [39]. However, we also remark that this value is to be considered as purely indicative, due to the possible macro- and micro-scale variability of massive serpentinites (for example, relative core vs. rim development, bastite abundance, as well as frequency of sigmoidal fibrous microveins, see below). Figure 6a,b refer to lens-shaped portions occurring in foliated serpentines and show the almost complete disappearance of mesh cores due to preferential pressure solution and the progressive evolution of mesh rims to isoriented lizardite "ribbons". The other consequence of pressure solution processes is the pervasive precipitation of fibrous and pseudofibrous serpentine in veinlets, corridors, shear zones, from micrometer to meter thick. Figure 6c shows a typical example of chrysotile sigmoidal veinlets, cutting both mesh, hourglass and bastites pseudomorphic textures. Chrysotile fibrous veins are easily recognizable at the petrographic observation due to their exceptionally high birefringence color, up to red–light blue tones. Figure 6d refers to a different kind of serpentine vein, predominantly consisting of polygonal serpentine fibers and resulting from crack and seal crystallization mechanisms [56,62]. As stated above, other common serpentine veins are those formed by predominant antigorite, in tiny lamellae elongated parallel to shear direction (Figure 7). We remark therefore that the extent of pressure solution processes and the subsequent precipitation of new serpentines are fundamental to determine the overall fiber content in a specific serpentinite outcrop.

Both MS and FS lithotypes may be affected by brittle fracturing, resulting into cataclastic serpentinites CS (Figure 8a), where fragments of meshes (Figure 8b), bastites (Figure 8c), and serpentine veins are embedded within a fine-to-ultrafine matrix of serpentine grains. Usually, cataclastic serpentinites (CS) are poorly coherent. Therefore, if cataclasis has involved serpentinites with abundant fibrous veins, we may reasonably expect, for this kind of lithotype, the highest potential of fiber release.

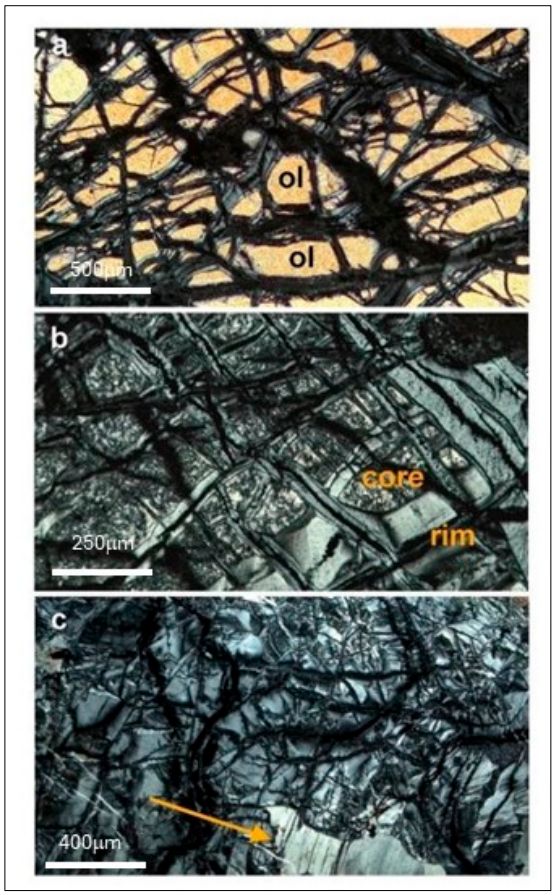

Figure 5. Crossed nicols, polarizing microscope images of massive serpentinites: (**a**) partially hydrated peridotite, with lizardite rims (gray) and preserved olivine cores (yellow); (**b**) mesh texture in pseudomorphic serpentinites, consisting of lizardite rims and polyphasic serpentine cores; (**c**) hourglass pseudomorphic texture, mainly formed by lizardite "sectors"; the orange arrow points to a bastitic lamella, formed by pyroxene serpentinization.

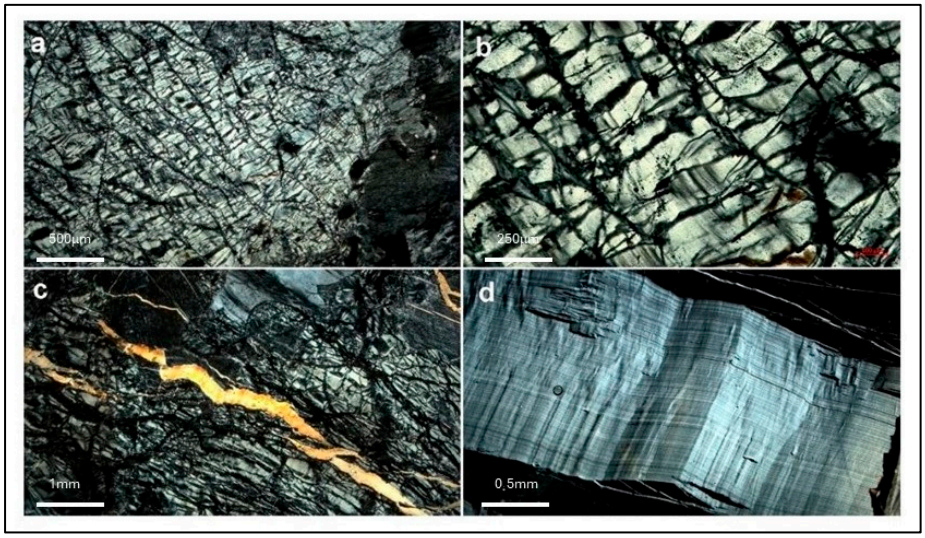

Figure 6. Crossed nicols, polarizing optical microscope images of foliated serpentinites: (**a**,**b**) deformed mesh texture, with preferential pressure solution of cores and development of lizardite "ribbon" textures; (**c**) typical sigmoidal chrysotile veinlets, cutting previous pseudomorphic textures; (**d**) crack-and-seal serpentine vein with a common association of polygonal serpentine and chrysotile.

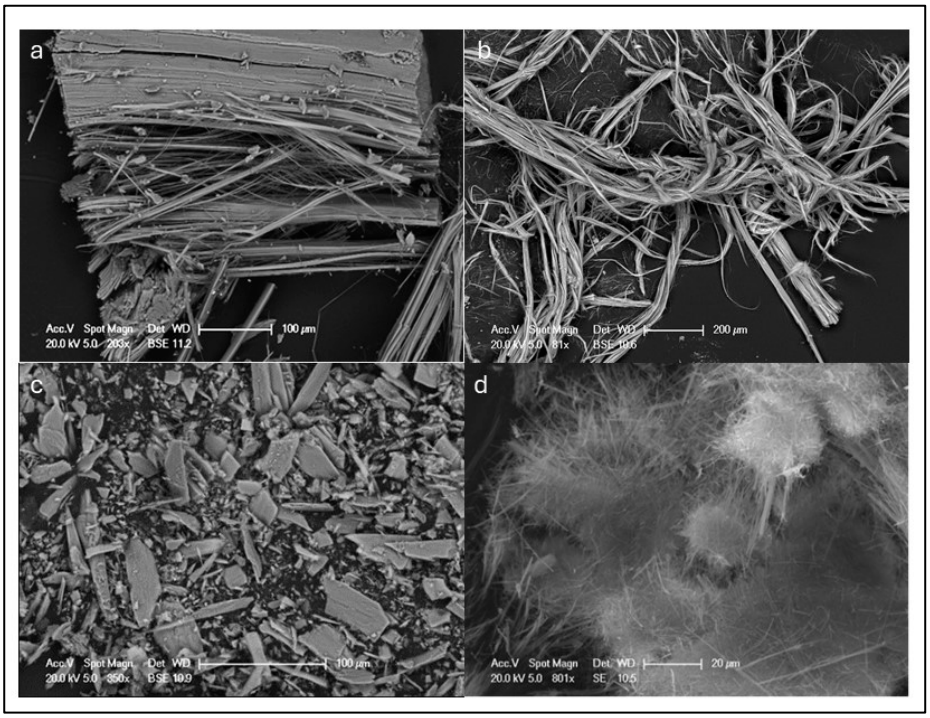

Figure 7. SEM images (both backscattered, BSE, and secondary electrons, SE) of different pale green veins and shear zones, surrounding massive dark green serpentinites: (**a**) Chrysotile isoriented fibers from a monomineralic sigmoidal vein, up to 500 µm thick; (**b**) Chrysotile long fibers from a larger shear zone; (**c**) Antigorite lamellae from a splintery pale green vein; (**d**) Tremolite fibers in irregular veins and patches within cataclastic serpentinites.

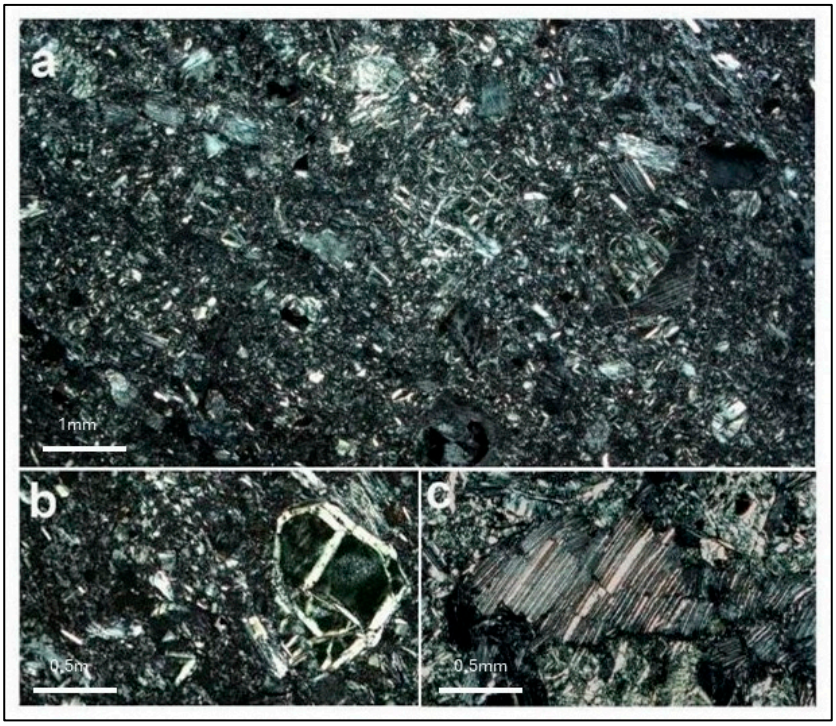

Figure 8. Crossed nicols, polarizing microscope images of cataclastic serpentinites: (**a**) clasts of serpentine pseudomorphs (meshes and bastites), embedded within a fine-to-ultrafine serpentine matrix; (**b**,**c**) details of mesh and bastite clasts, respectively.

3.2. Grinding and FTIR Tests Results

Abrasion test, density (g/cm^3), bulk density (g/cm^3), relative density (%), and Release Index results are shown in Table 2.

Table 2. Abrasion test, density (g/cm^3), bulk density (g/cm^3), relative density (%), and Release Index results from the FTIR analysis related to the collected samples.

Sample	Lithotype	Starting Weight (g)	Final Weight (g)	Powder Weight (g)	Density (g/cm^3)	Bulk Density (g/cm^3)	Relative Density (%)	Release Index (-)
MtRog_01	MS	500.62	478.07	22.55	2.70	2.65	98	0.01
MtRog_02	CS	500.32	469.05	31.27	2.75	2.54	92	0.76
MtRog_03	MS	500.20	462.20	38.00	2.66	2.56	96	0.20
MtRog_04	CS	500.50	437.86	62.64	2.71	2.52	93	0.66
MtRog_05	FS	500.15	410.70	89.45	2.73	2.54	93	0.53
MtRog_06	FS	500.22	360.86	139.36	2.67	2.49	93	0.00
MtRog_07	CS	500.48	432.62	67.86	2.71	2.59	95	0.58
MtRog_08	FS	500.12	487.50	12.62	2.68	2.60	97	0.00
MtRog_09	MS	500.34	475.26	25.08	2.72	2.61	96	0.00
MtRog_10	FS	500.65	479.80	20.85	2.81	2.65	94	0.01
MtRog_11	MS	500.23	481.10	19.13	2.70	2.60	96	0.00

The samples are relatively constant in terms of density, with minimum and maximum values of 2.66 g/cm^3 (MtRog_03) and 2.75 g/cm^3 (MtRog_02), respectively. The same considerations can be extended to the bulk density results, with the minimum value equal to 2.49 g/cm^3 (MtRog_06) and the maximum value equal to 2.65 g/cm^3 (MtRog_01 and MtRog_10). Relative density values range from 92% (MtRog_02) to 98% (MtRog_01). The last column in Table 2 reports the RI determinations obtained by FTIR quantitative analysis on the powders released during wear tests. The highest values of RI are always related to cataclastic serpentinites (CS), with values ranging from 0.58 to 0.76 (Table 2 and Figure 9). It is worth noting that massive serpentinites (MS) systematically provide the lowest values of the release index (often close to zero), indicating that this kind of lithology does not release asbestos fibers. The case of foliated samples is more complex, showing both values typical of massive serpentinites (RI close to zero) and higher values, approaching those of cataclastic serpentinites. We suggest that this variability reflects the strong heterogeneity of hand samples, where massive lenses of serpentinite are surrounded by fibrous, splintery veins, at any scale (from the outcrop to the micron scale).

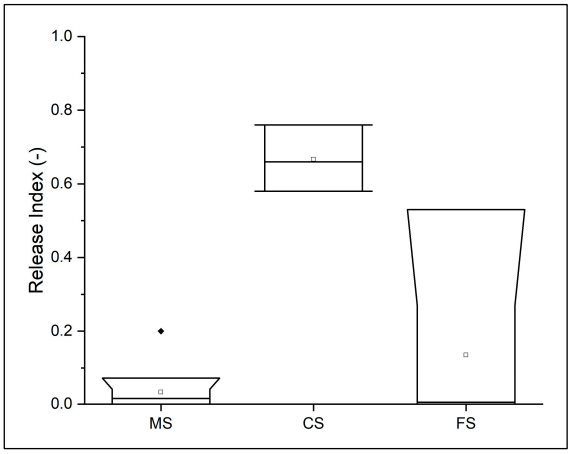

Figure 9. Boxplots of FTIR quantitative data showing Release Index in the three main data acquisition lithotypes ("MS"—Massive Serpentinites, "CS"—Cataclasite, and "FS"—Serpentine veins). The box represents data within the first and the third quartiles; the dot symbol represents the mean value; the line within the box represents the median value.

For comparison, the Release Index values obtained for massive samples from different outcrops (Calabria serpentinites) and using a different counting method (traditional SEM fiber counts on the released powder fraction) are reported in Table 3. These results confirm that, independently from the outcrops and the methodological method, undeformed massive serpentines have a very low RI (Figure 10).

Table 3. Abrasion test, relative density (%), and Release Index results from the optical analysis related to the Calabria collected samples.

Sample	Lithotype	Starting Weight (g)	Final Weight (g)	Powder Weight (g)	Release Index (-)
1S	MS	502.20	394.13	108.07	0.03
2S	MS	501.80	473.06	28.74	0.00
3S	MS	503.40	449.00	54.40	0.04
4S	MS	509.77	408.07	101.7	0.07
5S	MS	503.74	487.11	16.63	0.00
6S	MS	506.07	420.63	85.44	0.04
7S	MS	510.80	421.15	89.65	0.01
8S	MS	505.37	483.54	21.83	0.00
9S	MS	505.50	472.50	33.00	0.02
10S	MS	502.40	480.04	22.36	0.03

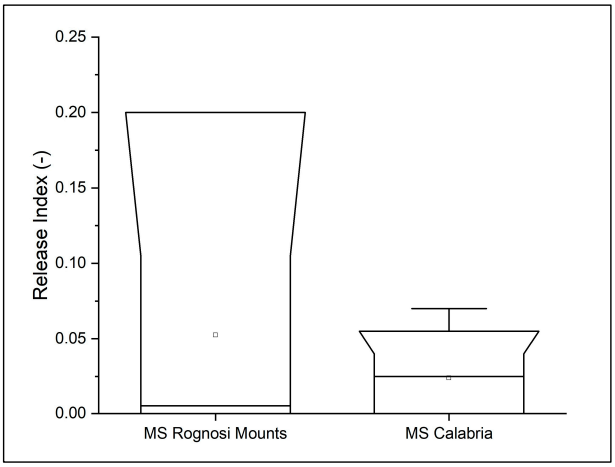

Figure 10. Boxplots of FTIR data showing Release Index in the two different study areas considered ("MS Rognosi Mounts" and "MS Calabria"). The box represents data within the first and the third quartiles; the dot symbol represents the mean value; the line extending parallel from the box is the whisker in the range 10–90; the line within the box represents the median value.

4. Discussion

In this paper, we studied a set of serpentinite samples characterized by different serpentinization degree, deformation extent, and style, to establish their potential asbestos hazard. Preliminary investigation allowed us to identify three main lithotypes that are common in every retrograde serpentinite outcrop around the world: (1) massive pseudomorphic serpentinites; (2) foliated serpentinites, formed by pressure-solution deformation mechanisms, followed by fibrous serpentine precipitation in veins and shear corridors; (3) cataclastic serpentinites, dominated by brittle fracturing and grain size reduction. It is worth noting that brittle cataclastic deformation may affect both massive serpentinites (where chrysotile fibers are ultrafinely associated to non-fibrous serpentines) and foliated serpentinites (where chrysotile fibers occur in monophasic veins). We remark that, differently from MS and CS, foliated serpentinites (FS) are characterized by a strongly heterogeneous microstructure and mineralogy, being formed by pods and lenses of MS (ultrafine compact association of different serpentine polymorphs) and monomineralic

veins and corridors (that may consist of chrysotile or chrysotile + polygonal serpentine or antigorite). This heterogeneity occurs at the outcrop scale (with chrysotile fibrous veins up to 5 cm wide) down to the micron scale (e.g., see Figure 6c). This feature may strongly complicate sample representativeness. In all cases, our study confirms that the amount, distribution, and release potential of chrysotile fibers in the environment is mostly driven by deformation style and extent, with a hypothetical increasing hazard scale from massive serpentinite, foliated serpentinite, and cataclastic serpentinite. In this context, a first attempt towards the assessment of the asbestos hazard related to a generic serpentinite outcrop has been carried out by Gaggero et al. [22], with a modified version of the UNI EN ISO 14689-1 protocol ("Indagini e prove geotecniche—Identificazione e classificazione delle rocce") [22] that considers the geometry relationships between vein networks and the undisturbed outcrop volume. These authors suggest a protocol that overcomes the Italian guidelines [19] and that includes the engineering geology and geological characterization of outcrops by mineralogical, petrological, and geotechnical analyses, with the quantitative determination of the asbestos in bulk samples. As stated in the Section 1, however, a reliable hazard assessment of NOA should consider the number of fibers that could actually be released in the environment. This can be performed through quantitative estimates of the released powders after normalized wear tests (release index determination).

Systematic determinations of the Release Index for a representative set of serpentinite samples were not available so far. Our paper filled this gap, providing a comprehensive RI dataset for the main lithotypes occurring in retrograde serpentinites. RI results confirm our hypothetical hazard scale, with the highest RI for cataclastic serpentinites showing abundant "clasts" of fibrous and splintery veins (i.e., foliated serpentinites that experienced subsequent brittle deformation). We remark that all CS samples always provided high RI values, well above the normative limits (RI threshold equal to 0.1) [19]. Conversely, the RI data for FS are quite inhomogeneous, with values close to zero or close to those expected for CS. This variability is probably due to the intrinsic heterogeneity of FS samples, as detailed above. The most important result, however, comes from massive, undeformed serpentinites. In fact, disregarding the actual occurrence of chrysotile fibers in pseudomorphic textures (up to 25%), massive serpentinites do not release fibers. This means that a homogeneous and undeformed outcrop of massive serpentinite could be excavated and quarried with close to zero hazard. The absence of asbestos fibers in the released inhalable powders can be explained by considering the ultrafine, close association of fibrous and non-fibrous serpentines. In other words, the compact and interpenetrated nanostructure of chrysotile fiber + lizardite lamellae in meshes and bastites hampers the release of single isolated (and then inhalable) fibers, even during wearing.

Future study will be dedicated to the realization of a detailed standardized procedure for asbestos hazard assessment in retrograde serpentinitic outcrops. The study will include a mesoscale quantitative analysis with areal and volumetric estimations of MS, FS, and CS. Starting from a terrestrial photogrammetric survey [63], the interpretation of the produced digital surface model and orthophoto will allow to carry out a geostatistical analysis of joint number, length, and frequency. It will be based on the 'P' system, introduced by Dershowitz and Herda [64], with the aim of proposing a possible hazard threshold on asbestos fibers release between massive and cataclastic outcrops. Moreover, the procedure for asbestos hazard assessment will include: (1) petrographic investigation of the main lithologies; (2) mineralogical characterization of fibrous and pseudofibrous veins; (3) asbestos fibers identification and quantification in released inhalable fraction, only for the most critical sites. Such a reasonable and non-alarmistic approach represents the only viable way to obtain an overall picture of the potential hazard of serpentinite outcrops, expanding our attention and our experimental efforts from the hand-sample to the meso- and regional scales.

5. Conclusions

This study provides new insights into the correlation among mineralogy, petrography, deformation features of a serpentinite outcrop, and its asbestos Release Index. Preliminary

geological and minero-petrographic survey of the study area allows us to identify three main lithotypes with different serpentinization degree, deformation extent, and style. We remark that the three lithotypes (i.e., massive, foliated, and cataclastic serpentinites) occur in all retrograde serpentinites around the world, and they can therefore be considered as a sort of representative "end members", at least for the purpose of this paper, which is the evaluation of asbestos hazard in the NOA context.

The most important conclusion of our study is the experimental demonstration that undeformed massive serpentinites do not represent an asbestos hazard, since they have an RI systematically close to zero, disregarding the fact that they contain up to 25% chrysotile fibers. This specific result should represent the common starting point to establish the best procedure for accurate assessment of asbestos hazard in retrograde serpentinite outcrops. Our results strengthen previous studies that have suggested mesoscale geomechanical analysis as the most reliable way for asbestos hazard evaluation.

Author Contributions: Conceptualization, M.I. and C.V.; methodology, M.I. and C.V.; software, M.I. and L.M.; validation, M.I. and C.V.; formal analysis, M.I. and C.V.; investigation, F.B., R.S., P.C. and C.V.; resources, C.V.; data curation, L.M. and C.V.; writing—original draft preparation, L.M., G.G. and C.V.; writing—review and editing, L.M., G.G., C.V. and R.S.; visualization, L.M., G.G. and C.V.; supervision, C.V.; project administration, C.V.; funding acquisition, C.V. All authors have read and agreed to the published version of the manuscript.

Funding: This research received no external funding.

Data Availability Statement: All data generated or analyzed for this study are included in this article, and the related datasets are available from the corresponding author upon reasonable request.

Acknowledgments: We would like to express our gratitude for the support provided by editor. We appreciate the valuable comments from the two reviewers, which have improved this manuscript.

Conflicts of Interest: The authors declare no conflicts of interest.

References

1. Ross, M.; Nolan, R.P. History of asbestos discovery and use and asbestos-related disease in context with the occurrence of asbestos within ophiolite complexes. In *Ophiolite Concept and the Evolution of Geological Thought*; Dilek, Y., Newcomb, S., Eds.; The Geological Society of America, Inc.: Boulder, CO, USA, 2003.
2. Strohmeier, B.R.; Huntington, J.C.; Bunker, K.L.; Sanchez, M.S.; Allison, K.; Lee, R.J. What is asbestos and why is it important? Challenges of defining and characterizing asbestos. *Int. Geol. Rev.* **2010**, *52*, 801–872. [CrossRef]
3. Militello, G.M.; Gaggero, L.; La Maestra, S. Asbestiform amphiboles and cleavage fragments analogues: Overview of critical dimensions, aspect ratios, exposure and health effects. *Minerals* **2021**, *11*, 525. [CrossRef]
4. Bolan, S.; Kempton, L.; McCarthy, T.; Wijesekara, H.; Piyathilake, U.; Jasemizad, T.; Padhye, L.P.; Zhang, T.; Rinklebe, J.; Wang, H.; et al. Sustainable management of hazardous asbestos-containing materials: Containment, stabilization and inertization. *Sci. Total Environ.* **2023**, *881*, 163456. [CrossRef] [PubMed]
5. Zaccagnini, E.; Marroni, M. Airborne dispersion of asbestos fibers from serpentinites: A simulation on ophiolites of pievescola area (Tuscany, Italy). *Ofioliti* **2013**, *38*, 75–87. [CrossRef]
6. Marabini, A.; Fonda, A.; Plescia, P. *Amianto Manuale Tecnico e Operativo, Consiglio Nazionale delle Ricerche*; Italy Press: Rome, Italy, 2002.
7. Marian, N.M.; Giorgetti, G.; Magrini, C.; Capitani, G.C.; Galimberti, L.; Cavallo, A.; Salvini, R.; Vanneschi, C.; Viti, C. From hazardous asbestos containing wastes (ACW) to new secondary raw material through a new sustainable inertization process: A multimethodological mineralogical study. *J. Hazard Mater.* **2021**, *413*, 125419. [CrossRef] [PubMed]
8. Vergani, F.; Galimberti, L.; Marian, N.M.; Giorgetti, G.; Viti, C.; Capitani, G. Thermal decomposition of cement–asbestos at 1100 °C: How much "safe" is "safe". *J. Mater. Cycles Waste Manag.* **2022**, *24*, 297–310. [CrossRef]
9. Virta, R.L. *Asbestos: Geology, Mineralogy, Mining, and Uses*; US Department of the Interior, US Geological Survey: Washington, DC, USA, 2002.
10. IARC. Some inorganic and organometallic compounds. In *IARC Monographs on the Evaluation of Carcinogenic Risk of Chemicals to Man*; World Health Organization: Geneva, Switzerland, 1973; Volume 2, pp. 1–181.
11. Wagner, J.C.; Sleggs, C.A.; Marchend, P. Diffuse pleural mesothelioma and asbestos exposure in the North Western Cape Province. *Br. J. Ind. Med.* **1960**, *17*, 260–271. [CrossRef] [PubMed]
12. Selikoff, I.J.; Churg, J.; Hammond, E.C. Relation between exposure to asbestos and mesothelioma. *N. Engl. J. Med* **1965**, *272*, 560–565. [CrossRef]
13. Skinner, H.C.W.; Ross, M.; Frondel, C. *Asbestos and Other Fibrous Materials: Mineralogy, Crystal Chemistry, and Health Effects*; Oxford University Press: New York, NY, USA, 1988.

14. Barrett, J.C.; Lamb, P.W.; Wiseman, R.W. Multiple mechanisms for the carcinogenic effects of asbestos and other mineral fibers. *Environ. Health Perspect.* **1989**, *81*, 81–89. [CrossRef]
15. Guthrie, G.D.; Mossman, B.T. *Health Effects of Mineral Dust*; Mineralogical Society of America, Ed.; Reviews in Mineralogy; P.H. Ribbe Series; Walter de Gruyter: Berlin, Germany, 1993.
16. Dela Cruz, C.S.; Tanoue, L.T.; Matthay, R.A. Lung cancer: Epidemiology, etiology, and prevention. *Clin. Chest Med.* **2011**, *32*, 605–644. [CrossRef]
17. Gualtieri, A.F. *Introduction. Mineral Fibres: Crystal Chemistry, Chemical–Physical Properties, Biological Interaction and Toxicity, Notes in Mineralogy*; European Mineralogical Union and the Mineralogical Society of Great Britain & Ireland: Twickenham, UK, 2017; pp. 1–15.
18. Decreto Legislativo (D.Lgs.) 17 March 1995. Available online: https://www.gazzettaufficiale.it/eli/id/1995/04/20/095G0149/sg (accessed on 27 June 2024).
19. Decreto Ministeriale (DM) 14 May 1996. Available online: https://www.gazzettaufficiale.it/eli/id/1996/10/25/096A6000/sg (accessed on 27 June 2024).
20. Lee, R.J.; Strohmeier, B.; Bunker, K.; Van Orden, D. Naturally occurring asbestos—A recurring public policy challenge. *J. Hazard. Mater.* **2008**, *153*, 1–21. [CrossRef] [PubMed]
21. Giacomini, F.; Boerio, V.; Polattini, S.; Tiepolo, M.; Tribuzio, R.; Zanetti, A. Evaluating asbestos fibre concentration in metaophiolites: A case study from the Voltri Massif and SestriVoltaggio Zone (Liguria, NW Italy). *Environ. Earth Sci.* **2010**, *61*, 1621–1639. [CrossRef]
22. Gaggero, L.; Crispini, L.; Isola, E.; Marescotti, P. Asbestos in natural and anthropic ophiolitic environments: A case study of geohazards related to the northern Apennine ophiolites (Eastern Liguria, Italy). *Ofioliti* **2013**, *38*, 29–40. [CrossRef]
23. Belardi, G.; Vignaroli, G.; Trapasso, F.; Pacella, A.; Passeri, D. Detecting asbestos fibres and cleavage fragments produced after mechanical tests on ophiolite rocks: Clues for the asbestos hazard evaluation. *J. Mediterr. Earth Sci.* **2018**, *10*, 63–78. [CrossRef]
24. Cossio, R.; Albonico, C.; Zanella, A.; Fraterrigo-Garofalo, S.; Avatenoe, C.; Compagnoni, R.; Turci, F. Innovative unattended SEM-EDS analysis for asbestos fiber quantification. *Talanta* **2018**, *190*, 158–166. [CrossRef]
25. Viti, C.; Mellini, M. Mesh textures and bastites in the Elba retrograde serpentinites. *Eur. J. Mineral.* **1998**, *10*, 1341–1359. [CrossRef]
26. Mevel, C. Serpentinization of abyssal peridotites at mid-ocean ridgesSerpentinisation des péridotites abysales aux dorsales océaniques. *Comptes Rendus Geosci.* **2003**, *335*, 825–852. [CrossRef]
27. Vignaroli, G.; Rossetti, F.; Belardi, G.; Billi, A. Linking rock fabric to fibrous mineralisation: A basic tool for the asbestos hazard. *Nat. Hazards Earth Syst. Sci.* **2011**, *11*, 1267–1280. [CrossRef]
28. Viti, C.; Mellini, M. Contrasting chemical compositions in associated lizardite and chrysotile in veins from Elba, Italy. *Eur. J. Mineral.* **1997**, *9*, 585–596. [CrossRef]
29. Lahondère, D.; Cagnard, F.; Wille, G.; Duron, J. Naturally occurring asbestos in an alpine ophiolitic complex (northern Corsica, France). *Environ. Earth Sci.* **2019**, *78*, 540. [CrossRef]
30. Rivero Crespo, M.A.; Pereira Gómez, D.; Villa García, M.V.; Gallardo Amores, J.M.; Sánchez Escribano, V. Characterization of Serpentines from Different Regions by Transmission Electron Microscopy, X-ray Diffraction, BET Specific Surface Area and Vibrational and Electronic Spectroscopy. *Fibers* **2019**, *7*, 47. [CrossRef]
31. Punturo, R.; Ricchiuti, C.; Bloise, A. Assessment of Serpentine Group Minerals in Soils: A Case Study from the Village of San Severino Lucano (Basilicata, Southern Italy). *Fibers* **2019**, *7*, 18. [CrossRef]
32. Lewis, I.R.; Chaffin, N.C.; Gunter, M.E.; Griffiths, P.R. Vibrational spectroscopic studies of asbestos and comparison of suitability for remote analysis. *Spectrochim. Acta Part A* **1996**, *52*, 315–328. [CrossRef]
33. Gualtieri, A.F.; Tartaglia, A. Thermal decomposition of asbestos and recycling in traditional ceramics. *J. Eur. Ceram. Soc.* **2000**, *20*, 1409–1418. [CrossRef]
34. Groppo, C.; Rinaudo, C.; Cairo, S.; Gastaldi, D.; Compagnoni, R. Micro-Raman spectroscopy for a quick and reliable identification of serpentine minerals from ultramafics. *Eur. J. Mineral.* **2006**, *18*, 319. [CrossRef]
35. Petriglieri, J.R.; Salvioli-Mariani, E.; Mantovani, L.; Tribaudino, M.; Lottici, P.P.; Laporte-Magoni, C.; Bersani, D. Micro-Raman mapping of the polymorphs of serpentine. *J. Raman Spectrosc.* **2015**, *46*, 953. [CrossRef]
36. Tarling, M.S.; Rooney, J.S.; Viti, C.; Smith, S.A.F.; Gordon, K.C. Distinguishing the Raman spectrum of polygonal serpentine. *J. Raman Spectrosc.* **2018**, *49*, 1978–1984. [CrossRef]
37. Petriglieri, J.R.; Laporte-Magoni, C.; Salvioli-Mariani, E.; Ferrando, S.; Tomatis, M.; Fubini, B.; Turci, F. Morphological and chemical properties of fibrous antigorite from lateritic deposit of New Caledonia in view of hazard assessment. *Sci. Total Environ.* **2021**, *777*, 146185. [CrossRef]
38. Petriglieri, J.R.; Barale, L.; Viti, C.; Ballirano, P.; Belluso, E.; Bruno, M.R.; Campopiano, A.; Cannizzaro, A.; Fantauzzi, M.; Gianchiglia, F.; et al. From field analysis to nanostructural investigation: A multidisciplinary approach to describe natural occurrence of asbestos in view of hazard assessment. *J. Hazard. Mater.* **2023**, *457*, 131754. [CrossRef]
39. Viti, C.; Giacobbe, C.; Gualtieri, A.F. Quantitative determination of chrysotile in massive serpentinites using DTA: Implications for asbestos determinations. *Am. Mineral.* **2011**, *96*, 1003–1011. [CrossRef]
40. Gualtieri, A.F.; Pollastri, S.; Bursi Gandolfi, N.; Ronchetti, F.; Albonico, C.; Cavallo, A.; Zanetti, G.; Marini, P.; Sala, O. Determination of the concentration of asbestos minerals in highly contaminated mine tailings: An example from abandoned mine waste of Crètaz and Èmarese (Valle d'Aosta, Italy). *Am. Mineral.* **2014**, *99*, 1233–1247. [CrossRef]

41. Bloise, A.; Catalano, M.; Critelli, T.; Apollaro, C.; Miriello, D. Naturally occurring asbestos: Potential for human exposure, San Severino Lucano (Basilicata, Southern Italy). *Environ. Earth Sci.* **2017**, *76*, 648. [CrossRef]
42. Decreto Legislativo (D.Lgs.) 152/2006. Available online: https://www.gazzettaufficiale.it/dettaglio/codici/materiaAmbientale (accessed on 27 June 2024).
43. Labagnara, D.; Patrucco, M.; Rossetti, P. Predictive assessment of the asbestos content in the Western Italian Alps: An essential tool for an effective approach to risk analysis and management in tunneling operations and muck reuse. *Environ. Earth Sci.* **2013**, *70*, 857–868. [CrossRef]
44. Lunardi, P.; Cassani, G.; Bellocchio, A.; Pennino, F. Naturally occurring asbestos in the Rocks belonging to Sestri–Voltaggio Zone (Liguria, Northern Italy). Excavation Railway tunnels management–Terzo Valico dei Giovi. In Proceedings of the World Tunnel Congress 2017–Surface challenges–Underground Solutions, Bergen, Norway, 9–15 June 2017.
45. Boccaletti, M.; Guazzone, G. Il microcontinente sardo-corso come un arco residuo di un sistema arco-fossa miocenico. In *Paleogeografia del Terziario Sardo Nell'ambito del Mediterraneo Occidentale*; Maxia, C., Cerchi, A., Eds.; Rendiconti del Seminario delle Facoltà di Scienze dell'Università di Cagliari; Graficoop: Bologna, Italy, 1974; Volume 43, pp. 57–68.
46. Principi, G.; Treves, B. Il sistema corso-appenninico come prisma d'accrezione. Riflessi sul problema generale del limite Alpi-Appennini. *Mem. Della Soc. Geol. Ital.* **1984**, *28*, 549–576.
47. Ricci Lucchi, F. The Oligocene to recent foreland basins of the Northern Apennines. In *Foreland Basins*; Allen, P.A., Homewood, P., Eds.; Blackwell Scientific: Oxford, UK, 1986; Volume 8, pp. 105–139.
48. Marzini, L.; D'Addario, E.; Papasidero, M.P.; Chianucci, F.; Disperati, L. Influence of Root Reinforcement on Shallow Landslide Distribution: A Case Study in Garfagnana (Northern Tuscany, Italy). *Geosciences* **2023**, *13*, 326. [CrossRef]
49. Plesi, G.; Galli, M.; Daniele, G. The Monti Rognosi Ophiolitic Unit (cfr. Calvana Unit Auct.) paleogeographic position in the External Ligurian Domain, relationships with the tectonic units derived from the Adriatic margin. *Boll. Della Soc. Geol. Ital.* **2002**, *1*, 273–284.
50. de Capoa, P.; D'Errico, M.; Di Staso, A. The succession of the Val Marecchia Nappe (Northern Apennines, Italy) in the light of new field and biostratigraphic data. *Swiss J. Geosci.* **2015**, *108*, 35–54. [CrossRef]
51. Vespasiano, G.; Muto, F.; Apollaro, C. Geochemical, Geological and Groundwater Quality Characterization of a Complex Geological Framework: The Case Study of the Coreca Area (Calabria, South Italy). *Geosciences* **2021**, *11*, 121. [CrossRef]
52. Zakrzewska, A.M.; Capone, P.P.; Iannò, A.; Tarzia, V.; Campopiano, A.; Villella, E.; Giardino, R. Calabrian ophiolites: Dispersion of airborne asbestos fibers during mining and milling operations. *Period. Mineral.* **2008**, *77*, 27–34. [CrossRef]
53. Bloise, A.; Critelli, T.; Catalano, M.; Apollaro, C.; Miriello, D.; Croce, A.; Barrese, E.; Liberi, F.; Piluso, E.; Rinaudo, C.; et al. Asbestos and other fibrous minerals contained in the serpentinites of the Gimigliano-Mount Reventino Unit (Calabria, S-Italy). *Environ. Earth Sci.* **2014**, *71*, 3773–3786. [CrossRef]
54. Bloise, A.; Belluso, E.; Critelli, T.; Catalano, M.; Apollaro, C.; Miriello, D.; Barrese, E. Amphibole asbestos and other fibrous minerals in the meta-basalt of the Gimigliano-Mount Reventino Unit (Calabria, south-Italy). *Rend. Online Della Soc. Geol. Ital.* **2012**, *21*, 847–848.
55. Regione Toscana–DB Geologico. Available online: http://www502.regione.toscana.it/geoscopio/geologia.html (accessed on 27 June 2024).
56. Tarling, M.S.; Smith, S.A.F.; Scott, J.M.; Rooney, J.S.; Viti, C.; Gordon, K.C. The internal structure and composition of a plate-boundary-scale serpentinite shear zone: The Livingstone Fault, New Zealand. *Solid Earth* **2019**, *10*, 1025–1047. [CrossRef]
57. Bellopede, R.; Clerici, C.; Marini, P.; Zanetti, G. Rocks with Asbestos: Risk Evaluation by Means of an Abrasion Test. *Am. J. Environ. Sci.* **2009**, *5*, 501–507.
58. Olori, A.; Di Pietro, P.; Campoiano, A. Preparation of ultrapure Kbr method for FTIR quantitative analysis. *Int. J. Sci. Acad. Res.* **2021**, *2*, 1015–1020.
59. Marzini, L.; Ciofini, D.; Agresti, J.; Ciaccheri, L.; D'Addario, E.; Disperati, L.; Siano, S.; Osticioli, I. Exploring the Potential of Portable Spectroscopic Techniques for the Biochemical Characterization of Roots in Shallow Landslides. *Forests* **2023**, *14*, 825. [CrossRef]
60. Accardo, G.; Cioffi, R.; Colangelo, F.; D'Angelo, R.; De Stefano, L.; Paglietti, F. Diffuse Reflectance Infrared Fourier Transform Spectroscopy for the Determination of Asbestos Species in Bulk Building Materials. *Materials* **2014**, *7*, 457–470. [CrossRef] [PubMed]
61. Wu, S.; He, M.; Yang, M.; Zhang, B.; Wang, F.; Li, Q. Near-Infrared Spectroscopy Study of Serpentine Minerals and Assignment of the OH Group. *Crystals* **2021**, *11*, 1130. [CrossRef]
62. Andreani, M.; Baronnet, A.; Boullier, A.M.; Gratier, J.P. A microstructural study of a "crack-seal" type serpentine vein using SEM and TEM techniques. *Eur. J. Mineral.* **2004**, *16*, 585–595. [CrossRef]
63. Salvini, R.; Riccucci, S.; Gullì, D.; Giovannini, R.; Vanneschi, C.; Francioni, M. Geological application of UAV photogrammetry and terrestrial laser scanning in marble quarrying (Apuan Alps, Italy). In *Engineering Geology for Society and Territory*; Springer: Cham, Switzerland, 2015; Volume 5, pp. 979–983.
64. Dershowitz, W.S.; Herda, H. Interpretation of fracture spacing and intensity. In Proceedings of the 33rd US Symposium on Rock Mechanics (USRMS), Santa Fe, NM, USA, 3–5 June 1992; Balkema, A.A., Ed.;

Disclaimer/Publisher's Note: The statements, opinions and data contained in all publications are solely those of the individual author(s) and contributor(s) and not of MDPI and/or the editor(s). MDPI and/or the editor(s) disclaim responsibility for any injury to people or property resulting from any ideas, methods, instructions or products referred to in the content.